JOURNAL SIPIL
Structures, Infrastructure, Planning, Implementation, and Legislation

3D FEM Assessment of Rainfall-Induced Stability of Residual Soil Slopes under Extreme Rainfall

Azizah Rokhmawati[1]*, Meny Sriwati[2], Makmur[3], Muhammad Riski[4], & M. Nuril Anwar Habiby[5]
[1]*Universitas Islam Malang, Indonesia, [2]STITEK Dharma Yadi Makassar, Indonesia, [3]Politeknik Negeri Fakfak, Indonesia, [4]Politeknik Negeri Padang, Indonesia, [5]Universitas Negeri Semarang, Indonesia
*Co e-mail: rokhmawatiazizah@gmail.com[1]

Article Information
Received: July 04, 2026
Revised: October 16, 2026
Online: October 26, 2026

Keywords
Residual Soil, Slope Stability, 3D Finite Element Method, Rainfall Infiltration

ABSTRACT
Hilly areas underlain by tropical residual soil are susceptible to rainfall-induced slope failure as infiltration reduces matric suction and soil shear strength. This study investigates three-dimensional (3D) slope stability using the finite element method (FEM), coupling transient unsaturated seepage analysis with the shear strength reduction method (SRM) to evaluate time-dependent factors of safety (FoS). Four representative slope profiles (25°–38° inclination and 8–15 m height) in West Sumatra were modeled using laboratory-derived residual soil parameters, including effective cohesion, friction angle, saturated permeability, and soil-water characteristic curves. The slopes were subjected to a synthetic 72-hour extreme rainfall event with a peak intensity of 45 mm/h. Results showed that pore-water pressure increased from an initial matric suction of −55 kPa to near-zero or slightly positive values within 24–48 hours. Consequently, FoS decreased by 25.0–31.9% compared with dry conditions. The steepest profile (38°, 15 m height) reached a minimum FoS of 0.94 after approximately 40 hours, indicating potential failure. Critical slip surfaces occurred at depths of 1.5–3.0 m within the residual soil layer. Verification against 2D Bishop limit-equilibrium analysis was conducted under dry conditions. However, transient rainfall responses remain unvalidated. Therefore, findings indicate relative slope sensitivity rather than operational early-warning thresholds.

Keywords: *Residual Soil, Slope Stability, 3D Finite Element Method, Rainfall Infiltration*

INTRODUCTION

Rainfall-induced slope failure is one of the most frequent and destructive geotechnical hazards in tropical hilly regions, where thick mantles of weathered residual soil overlie less permeable saprolite or bedrock and are directly exposed to intense monsoonal rainfall (Sharma et al., 2021). Unlike transported or sedimentary soils, residual soils retain relict structure, cementation, and macropores inherited from the parent rock, giving them comparatively high shear strength and permeability in the unsaturated state but making them highly sensitive to strength loss once rainwater infiltration

DOI: http:// doi.org/10.69855/sipil.v2i2.698
Available online at website: https://gpijournal.com/index.php/sipil

This work is licensed under a Creative Commons Attribution 4.0 International license

eliminates matric suction (Rahardjo & Satyanaga, 2019; Satyanaga et al., 2025). This sensitivity is particularly critical during extreme rainy-season events, when sustained high-intensity rainfall can drive the wetting front through the entire residual soil layer within hours to a few days, triggering shallow translational or rotational failures on hillslopes used for roads, settlements, and agriculture (Chen et al., 2021; Kim et al., 2024).

Conventional slope stability assessment has historically relied on two-dimensional (2D) limit equilibrium methods (Bishop, Janbu, Spencer, or Morgenstern-Price), which are computationally efficient but require an a priori assumption of the critical cross-section and cannot represent the three-dimensional (3D) geometry of natural hillslopes, lateral confinement effects, or spatially variable rainfall infiltration (Oguz et al., 2022; Jiang et al., 2022). Three-dimensional finite element methods (3D FEM), by contrast, can simultaneously solve the coupled unsaturated seepage and stress-deformation problem over the full slope geometry and determine the factor of safety using the shear strength reduction method (SRM), in which the shear strength parameters are progressively reduced until the model reaches a state of numerical non-convergence corresponding to failure (Zhou et al., 2022; Bentley Systems Inc., 2023). Comparative studies have shown that 3D FEM/limit-equilibrium analyses typically produce factor-of-safety values within about 3-10% of 2D results for simple geometries, but diverge more substantially for slopes with complex topography, layered residual soil profiles, or spatially variable rainfall infiltration, where the additional lateral resistance and three-dimensional flow paths captured by 3D models become significant (Oguz et al., 2022; Das et al., 2023).

A substantial body of research has examined the coupling between rainfall infiltration and slope stability using numerical seepage-stress models. Rahimi et al. (2020) showed that the hydraulic properties of soil, particularly the saturated permeability and the shape of the soil-water characteristic curve (SWCC), strongly control the rate and depth of wetting-front advance and therefore the timing of failure. Garcia et al. (2021) used a multiphase coupled elasto-viscoplastic finite element formulation to simulate one-dimensional rainfall infiltration, while Zhan et al. (2020) developed an analytical solution for infiltration into an unsaturated infinite slope that has since been used to benchmark numerical models. More recent studies have extended these approaches to full 3D slope geometries: Zhou et al. (2022) presented a fully coupled hydro-mechanical 3D finite element analysis of rainfall-induced slope instability, and Kim et al. (2024) used 3D numerical modelling to reproduce a shallow landslide in weathered residual soil, finding that the depth and timing of failure were controlled by the interaction between rainfall intensity, initial groundwater level, and soil layering. For tropical residual soil specifically, Satyanaga et al. (2025) combined field instrumentation, laboratory testing, and PLAXIS 2D/GeoStudio numerical modelling to show that instrumentation-measured wetting-front depths matched numerical seepage predictions to within about 3-6%, supporting the reliability of coupled numerical approaches for residual soil slopes.

Despite this progress, three gaps remain for the problem addressed here. First, the 3D analyses of Zhou et al. (2022) and Kim et al. (2024) present, respectively, a general fully coupled hydro-mechanical formulation and the reproduction of a single shallow landslide in weathered residual soil; to the best of our knowledge, neither compares how slope inclination, slope height, and a toe cut change the time-dependent FoS of residual soil slopes under the same design storm. Second, the field-supported residual soil study of Satyanaga et al. (2025) relied on 2D numerical models, so lateral (3D) effects on the transient response were not examined. Third, most published coupled infiltration-stability studies for residual soil slopes remain two-dimensional (Oguz et al., 2022; Zhou et al., 2022), and the hydrological-stability relation (cumulative rainfall, wetting-front depth, pore-water pressure, and FoS over time) is rarely reported together for several slope geometries. West Sumatra is selected because

This work is licensed under a Creative Commons Attribution 4.0 International license

the region is underlain by 4–9 m thick residual soil derived from andesitic volcanic bedrock, experiences monsoonal rainfall with frequent high-intensity events, and has a documented history of rainfall-triggered landslides on hillslopes used for roads and settlements (Setiawan & Pratama, 2022). This setting differs from previously studied residual soil slopes in that the combination of steep topography (25°–38°), toe cuts for road construction, and extreme rainfall has not been analyzed using a fully coupled 3D FEM approach.

This study therefore aims to: (1) develop a 3D finite element model that couples transient unsaturated seepage with shear strength reduction stability analysis for residual soil slopes; (2) compare the time-dependent FoS of four slope profiles differing in inclination, height, and the presence of a toe cut under one 72-hour design rainfall event; and (3) quantify the relation among cumulative rainfall, wetting-front depth, pore-water pressure, minimum FoS, and critical slip depth, in order to characterize the dominant rainfall-induced failure mechanism and to provide a documented basis for future rainfall-threshold development. The study does not develop an operational early-warning threshold.

METHODS

1. Study Area and Slope Profiles

The study was conducted on hillslopes representative of a residual soil hilly area in West Sumatra, Indonesia, where andesitic volcanic bedrock has weathered into a mantle of clayey silt to silty clay residual soil, 5–9 m thick, overlying a saprolite transition zone. Four slope profiles were selected to represent the range of geometries observed in the study area: Profile A (25° inclination, 8 m height), Profile B (32°, 12 m), Profile C (38°, 15 m), and Profile D (28°, 10 m, with a toe road cut). The residual soil thickness and the elevation of the residual soil-saprolite boundary along each profile are 6.0 m and 2.0 m for Profile A, 7.5 m and 4.5 m for Profile B, 9.0 m and 6.0 m for Profile C, and 5.0 m and 3.0 m for Profile D, respectively, with boreholes BH-1 to BH-4 located at the crest, mid-slope, toe, and toe-cut of each profile (Figure 1 and Table 1). Undisturbed soil samples were collected from test pits and boreholes (12 samples: 8 from the residual soil layer at 1.5–3.5 m and 4 from the upper saprolite transition zone at 4.0–4.5 m, from BH-1 to BH-4; in profiles where the residual soil is 5–9 m thick, the 4.0–4.5 m samples represent the upper transition zone rather than the full saprolite) and subjected to index property tests, consolidated-drained triaxial compression tests, constant-head permeability tests, and filter-paper suction tests to establish the soil-water characteristic curve (SWCC).

Table 1. Geotechnical and hydraulic parameters of residual soil and saprolite layers used in the 3D FEM model

Parameter	Residual soil (upper)	Saprolite (lower)	Test method
Unit weight, γ (kN/m^3)	16.8	18.9	Core cutter
Effective cohesion, c' (kPa)	9.5	22.0	Triaxial CD
Friction angle, φ' (deg)	27.5	31.0	Triaxial CD
Saturated permeability, ksat (m/s)	3.6×10^{-6}	4.1×10^{-7}	Constant-head
Saturated water content, θs	0.46	0.38	Lab moisture-density
Air-entry value (kPa)	6.2	14.5	Filter paper / SWCC fit

This work is licensed under a Creative Commons Attribution 4.0 International license
Structures, Infrastructure, Planning, Implementation, and Legislation (SIPIL)
Vol. 02, No. 2, October 2026

The parameters in Table 1 represent the mean values obtained from 12 undisturbed soil samples, comprising eight samples from the residual soil layer and four from the saprolite transition zone. The measured ranges were 16.2–17.4 kN/m^3 for unit weight (γ), 8.6–10.4 kPa for effective cohesion (c'), 26.1–28.9° for effective friction angle (φ'), 2.9 × 10^{-6}–4.4 × 10^{-6} m/s for saturated hydraulic conductivity (k_{sat}), 0.44–0.48 for saturated volumetric water content (θ_s), and 5.4–7.1 kPa for air-entry value. The corresponding coefficients of variation were 8%, 12%, 7%, 15%, 4%, and 11%, respectively.

Additional parameters used in the model included residual volumetric water content (θ_r) of 0.08 for residual soil and 0.10 for saprolite; van Genuchten parameters α of 0.035 and 0.022 kPa^{-1} and n of 1.45 and 1.62 for residual soil and saprolite, respectively. The soil-water characteristic curves (SWCCs) were fitted using the filter paper method, yielding R^2 values of 0.96 for residual soil and 0.94 for saprolite. The effective Young's modulus (E') was set to 8,000 kPa for residual soil and 25,000 kPa for saprolite, while Poisson's ratios (ν') were 0.30 and 0.28, respectively. The elastic parameters were obtained from laboratory triaxial compression tests for residual soil and literature correlations for tropical residual soils and saprolite (Fredlund et al., 2021; Ng & Menzies, 2020).

2. 3D Finite Element Model and Rainfall Input

All analyses were performed using PLAXIS 3D V2023.1 (Bentley Systems Inc., 2023), in which transient seepage and deformation are solved in a coupled manner (Chai et al., 2020). Each slope profile was modeled in three dimensions in a domain of 60 × 40 × 25 m, discretized with 10-node tetrahedral elements (approximately 45,000 elements and 68,000 nodes; global element size 2.0 m). A refinement zone of 20 × 15 × 10 m along the slope surface and the anticipated failure region used an element size of 0.5 m; mesh quality was checked using aspect ratio and skewness (both < 0.85), and mesh sensitivity was tested for Profile C, where the difference in FoS between the medium and fine meshes was less than 2%, so the medium mesh was adopted. Figure 1 shows the 3D geometry, mesh and refinement zone, soil layers, boundary conditions, and rainfall boundary (Profile C). Soil behavior was represented by the Mohr-Coulomb model with the stiffness parameters listed in the note to Table 1. The unsaturated hydraulic conductivity function was described by the van Genuchten model fitted to the measured SWCC data (fitting parameters in the note to Table 1) (Fredlund et al., 2021; Ng & Menzies, 2020), and the contribution of suction to shear strength was represented using the Bishop effective stress approach with χ = S (degree of saturation). Mechanical boundary conditions consisted of fixed displacements at the base and roller boundaries at the lateral sides. The initial phreatic surface was set at 8.0 m below the ground surface from a steady-state seepage analysis calibrated against dry-season piezometer readings from four piezometers installed at BH-1 to BH-4 (August–September 2024). Hydraulic boundary conditions were an impermeable base and no-flow lateral sides, and the slope surface received the rainfall flux, with runoff allowed and no ponding. Convergence criteria were a maximum pore-pressure error of 0.01 m, a maximum displacement error of 0.001 m, a maximum of 100 SRM steps, and failure defined by non-convergence of the finite element solution.

The design rainfall was a 72-hour synthetic hyetograph with two intensity peaks (at 18 h and 40 h) and a maximum hourly intensity of 45 mm/h. It was derived from the records of Stasiun Meteorologi Minangkabau (BMKG), located approximately 25 km from the study site, with data obtained from the Indonesian Agency for Meteorology, Climatology, and Geophysics (BMKG) database for the period 2005–2024 (20 years) using frequency analysis of annual maximum daily rainfall fitted with the Gumbel distribution, verified by the Kolmogorov–Smirnov goodness-of-fit test at the 5% significance level, and disaggregated into an hourly pattern using the Mononobe method (Mononobe & Matsuo, 1949) with a

This work is licensed under a Creative Commons Attribution 4.0 International license

dual-peak temporal distribution for a 25-year return period. The peak intensity of 45 mm/h corresponds to the 95th percentile of observed hourly rainfall in the 20-year record; for the fitted Gumbel distribution, this intensity is approximately associated with a 25-year return period. The resulting hourly intensities and cumulative rainfall (total 480 mm over 72 h) are shown in Figure 2.

The rainfall was applied as a time-dependent flux boundary condition on the slope surface in a fully coupled transient seepage-deformation analysis, and the resulting pore-water pressure field at each time step was passed to the shear strength reduction (SRM) stability module, in which the effective cohesion and friction angle of every element were simultaneously divided by a trial strength reduction factor until the finite element model failed to converge, defining the factor of safety at that time step.

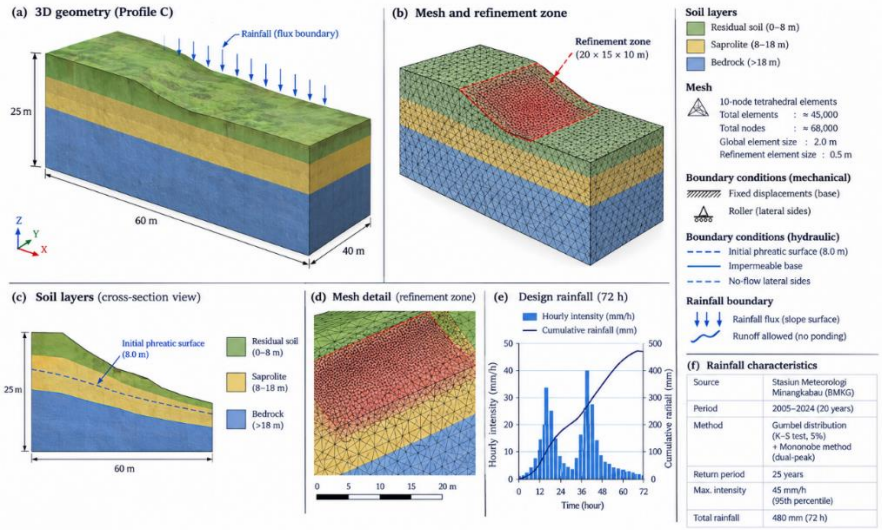


Figure 1. 3D finite element model of the slope: geometry, mesh and refinement zone, residual soil and saprolite layers, boundary conditions, and rainfall boundary (Profile C)

The design rainfall was a 72-hour synthetic hyetograph with two intensity peaks (at 18 h and 40 h) and a maximum hourly intensity of 45 mm/h. It was derived from the records of Stasiun Meteorologi Minangkabau (BMKG), located approximately 25 km from the study site, with data obtained from the Indonesian Agency for Meteorology, Climatology, and Geophysics (BMKG) database for the period 2005–2024 (20 years) using frequency analysis of annual maximum daily rainfall fitted with the Gumbel distribution, verified by the Kolmogorov-Smirnov goodness-of-fit test at the 5% significance level, and disaggregated into an hourly pattern using the Mononobe method with a dual peak temporal distribution for a return period of 25 years. The peak intensity of 45 mm/h was selected because it corresponds to the 95th percentile of observed hourly rainfall in the 20-year record and represents the intensity associated with the 25-year return period for this region. The hourly intensities and cumulative rainfall (total 480 mm over 72 h).

The rainfall was applied as a time-dependent flux boundary condition on the slope surface in a fully coupled transient seepage-deformation analysis, and the resulting pore-water pressure field at each time step was passed to the shear strength reduction (SRM) stability module, in which the effective cohesion and friction angle of every element were simultaneously divided by a trial strength reduction factor until the finite element model failed to converge, defining the factor of safety at that time step.

3. Verification, Calibration, and Validation

The numerical workflow was assessed in three distinct steps. (i) Verification: for the initial (dry/long-term) steady-state condition, the 3D FEM FoS was compared with 2D Bishop simplified limit-

This work is licensed under a Creative Commons Attribution 4.0 International license
Structures, Infrastructure, Planning, Implementation, and Legislation (SIPIL)
Vol. 02, No. 2, October 2026

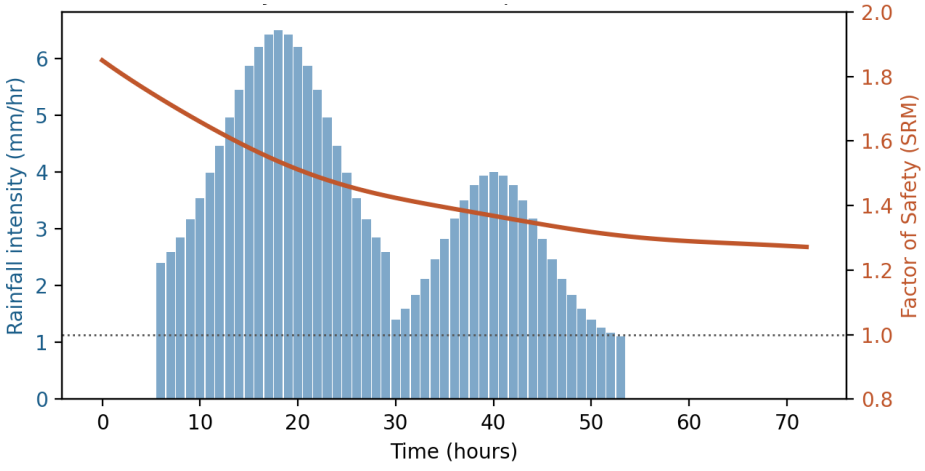
equilibrium calculations for the central cross-section of each profile with identical geometry and parameters. This checks the SRM implementation against an established method but says nothing about the transient rainfall response. (ii) Calibration: the initial phreatic surface was calibrated against dry-season piezometer readings, and the SWCC was fitted to filter-paper data; no parameter was adjusted to reproduce a measured rainfall response, so the calibration is limited to the initial condition. (iii) Plausibility check: the computed wetting-front depth was compared with field-instrumented wetting-front depths reported for comparable tropical residual soil slopes (Satyanaga et al., 2025). This comparison is a plausibility check rather than a validation for the four profiles analyzed, because no pore-water pressure monitoring data, rainfall records, or observed landslide events are available for the four specific slopes. The model should therefore be regarded as not fully validated for transient rainfall; validation against an observed failure, as in back-analysis studies (Wang et al., 2023), is left for future work. The model, verified only for the dry condition, was then run for each of the four profiles under the 72-hour design rainfall, with pore-water pressure and FoS recorded at 1-hour intervals.

RESULTS

1. Pore-Water Pressure Response to Rainfall Infiltration

During the 72-hour design storm, hourly rainfall intensity influenced the transient factor of safety (FoS) of Profile B (32°, H = 12 m). The FoS remained close to its initial (dry/long-term) value of approximately 1.61 during the first 6 hours, then declined steadily as the wetting front advanced, reaching a minimum of approximately 1.12 near hour 55, shortly after the second rainfall peak (Figure 2). The corresponding pore-water pressure profiles at 0, 12, 24, 48, and 72 hours (Figure 3) showed that the initial matric suction of approximately −55 kPa near the surface was progressively reduced as the wetting front advanced downward. By 48 hours, the wetting front had reached a depth of approximately 2.6 m, while near-zero to slightly positive pore-water pressure developed within the upper 1.5–2.0 m of residual soil by 72 hours.

The temporal responses of FoS, pore-water pressure at depths of 0.5, 1.0, 2.0, and 3.0 m below the slope surface, and wetting-front depth were evaluated for all four profiles (Figure 4). At the time of minimum FoS, the wetting-front depths reached 1.8 m for Profile A, 2.5 m for Profile B, 3.2 m for Profile C, and 2.3 m for Profile D. Meanwhile, pore-water pressure at the critical slip depth ranged from −5 to +2 kPa, indicating near-saturated conditions in the upper residual soil layer across all four profiles. Profile C, the steepest and tallest slope, exhibited the deepest wetting front (3.2 m) and the earliest minimum FoS at 40 hours. In contrast, Profile A, the gentlest and shortest slope, showed the shallowest wetting front (1.8 m) and the latest minimum FoS at 58 hours.



This work is licensed under a Creative Commons Attribution 4.0 International license

Figure 2. Rainfall intensity hyetograph and computed 3D factor of safety over a 72-hour extreme rainfall event (Profile B)

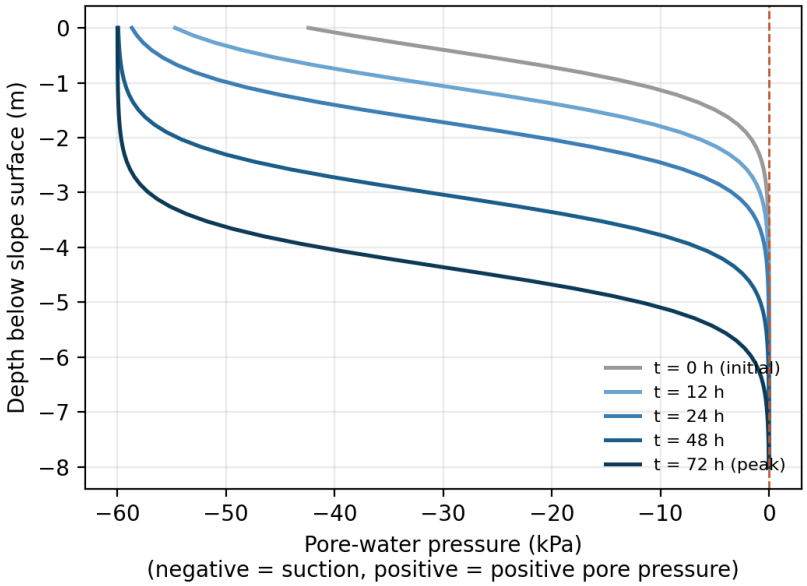


Figure 3. Pore-water pressure profile with depth at selected times during rainfall infiltration (Profile B)

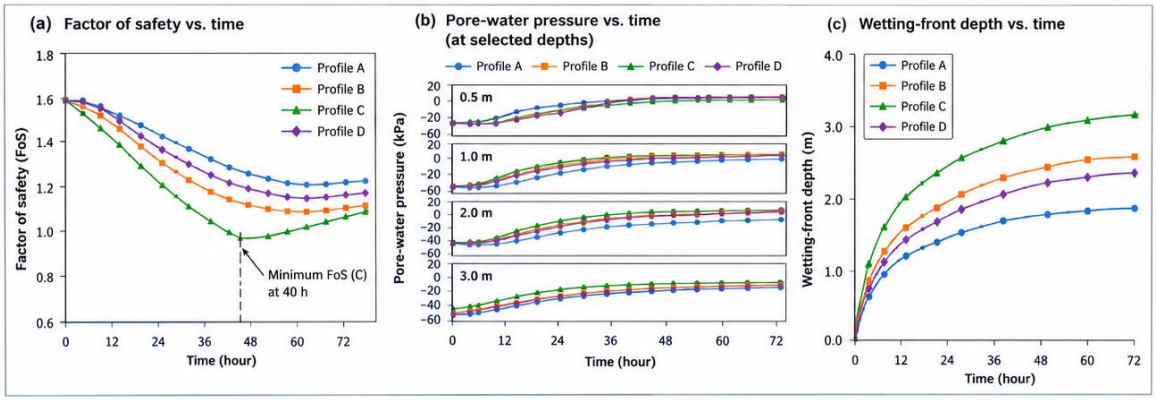


Figure 4. Time series for Profiles A–D: (a) factor of safety, (b) pore-water pressure at several depths, and (c) wetting-front depth

2. Factor of Safety Test Results Across Slope Profiles

The 3D FEM results for all four slope profiles under initial (dry/long-term) and extreme rainfall conditions included the minimum factor of safety (FoS), the time at which the minimum occurred, cumulative rainfall and wetting-front depth at that time, and the critical slip-surface depth identified through the strength reduction method (SRM). The FoS decreased by 25.0–31.9% relative to the initial (dry/long-term) condition, with reductions of 25.0%, 30.4%, 31.9%, and 30.3% for Profiles A–D, respectively. Profile C (38°, H = 15 m) reached a minimum FoS of 0.94, indicating predicted slope failure under the design storm, whereas Profiles A and D maintained FoS values above 1.0, although their safety margins were substantially reduced. For Profile C, the minimum FoS of 0.94 occurred at hour 40, when cumulative rainfall reached 320 mm and the wetting front extended to a depth of 3.2 m. The pore-water

This work is licensed under a Creative Commons Attribution 4.0 International license

pressure at the critical slip depth was +1.5 kPa, and the corresponding critical slip zone was identified through the SRM analysis (Figure 7).

Table 2. 3D FEM results for the four residual soil slope profiles: initial and minimum FoS, time to minimum FoS, cumulative rainfall and wetting-front depth at the minimum FoS, and critical slip depth

Profile	Initial FoS (dry)	FoS (rainy, min.)	FoS reduction (%)	Time to min. FoS (h)	Critical slip depth (m)	Cum. rainfall at min. FoS (mm)	Wetting-front depth at min. FoS (m)
A (25°, H=8m)	1.92	1.44	25.0%	58	1.5	410	1.8
B (32°, H=12m)	1.61	1.12	30.4%	55	2.2	390	2.5
C (38°, H=15m)	1.38	0.94	31.9%	40	3.0	320	3.2
D (28°, H=10m, toe cut)	1.55	1.08	30.3%	50	2.0	370	2.3

The results indicate that all four residual soil slope profiles experienced reductions in FoS under extreme rainfall, ranging from 25.0% to 31.9% relative to their initial (dry/long-term) condition (Table 2). Profile A, with the highest initial FoS (1.92), retained the highest minimum FoS (1.44), whereas Profile C, with the lowest initial FoS (1.38), declined to 0.94 and thus reached predicted failure under the design storm. Profiles B and D reached minimum FoS values of 1.12 and 1.08, respectively, indicating substantially reduced stability margins without crossing the nominal failure threshold. At the time of minimum FoS, cumulative rainfall ranged from 320 to 410 mm and wetting-front depths from 1.8 to 3.2 m. Profile C exhibited both the deepest wetting front (3.2 m) and the greatest FoS reduction (31.9%), highlighting its greater vulnerability to rainfall-induced instability. These results are deterministic estimates; uncertainty ranges were not quantified because a full probabilistic analysis was beyond the scope of the study.

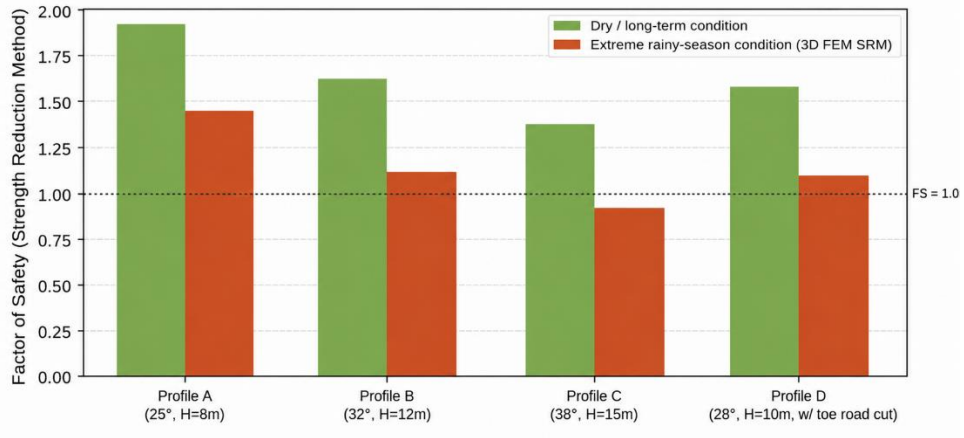


Figure 5. Comparison of factor of safety between dry/long-term and extreme rainfall conditions for four slope profiles

This work is licensed under a Creative Commons Attribution 4.0 International license

In all four profiles, the critical slip surface identified by the SRM analysis was shallow, ranging from 1.5 m to 3.0 m in depth. Because the residual soil is 5–9 m thick, slip depths of 1.5–3.0 m lie within the residual soil layer and above the residual soil–saprolite boundary, not on it. The elevation of that boundary relative to the slip surface in each profile is summarized in Table 3 and shown schematically in Figure 6: the residual soil–saprolite boundary is located at 2.0 m (Profile A), 4.5 m (Profile B), 6.0 m (Profile C), and 3.0 m (Profile D) above the toe level, so the critical slip surface remains 0.5–3.0 m above the boundary in all four profiles. The largest clearance occurs in Profile C (3.0 m slip depth versus 6.0 m boundary elevation, i.e., 3.0 m clearance), and the smallest in Profile A (1.5 m slip depth versus 2.0 m boundary elevation, i.e., 0.5 m clearance). Figure 6 illustrates a schematic cross-section through the 3D model showing the residual soil layer and the predicted critical slip surface for Profile C, and Figure 7 shows the displacement and shear strain distribution and the pore-water pressure at FoS = 0.94 for the same profile.

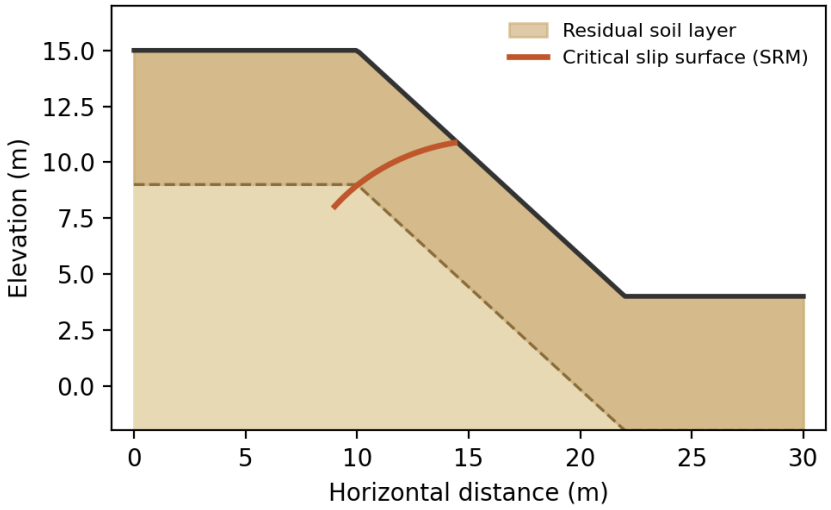


Figure 6. Schematic cross-section of the 3D finite element model showing the residual soil layer and the critical shallow slip surface (Profile C)

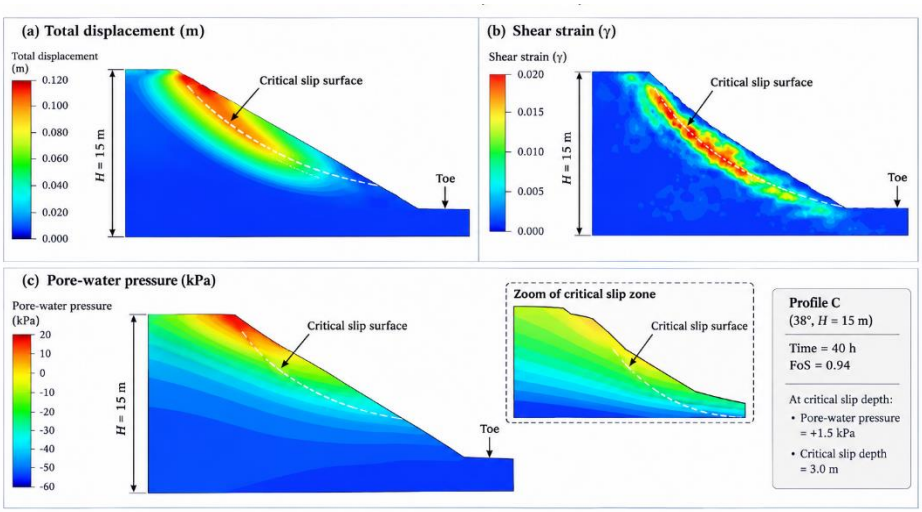


Figure 7. Profile C at 40 h (FoS = 0.94): total displacement or shear strain, critical slip zone, and pore-water pressure distribution

This work is licensed under a Creative Commons Attribution 4.0 International license
Structures, Infrastructure, Planning, Implementation, and Legislation (SIPIL)
Vol. 02, No. 2, October 2026

3. Comparison with 2D Limit Equilibrium Verification

For the initial (dry/long-term) condition, the 3D FEM factor of safety values were compared against 2D Bishop simplified limit-equilibrium calculations for the same central cross-section of each profile. The 3D FEM results were 4.8–8.6% higher than the corresponding 2D values, consistent with the additional lateral resistance captured by 3D analysis and with the range of 3–10% previously reported for comparisons between 3D and 2D slope stability methods (Oguz et al., 2022; Das et al., 2023); comparisons between finite element and limit-equilibrium tools have likewise been reported for road-cut slopes (Yudhistira et al., 2024). This comparison verifies the SRM implementation under dry conditions only. It does not validate the transient rainfall response, and it does not show that 3D analysis is more realistic than 2D analysis under rainfall, because no 2D transient rainfall analysis of the same four profiles was performed in this study. Consequently, it remains unknown whether a 2D assessment would overestimate or underestimate the minimum FoS under the design storm. The role of localized 3D infiltration effects, such as those expected at the toe cut of Profile D, remains a hypothesis to be tested in future work by comparing 2D and 3D pore-water pressure fields under identical rainfall input.

4. Sensitivity Analysis

A deterministic sensitivity analysis was performed for Profile C (38°, H = 15 m), the only profile that reached FoS < 1.0 under the design storm, to identify which parameters most strongly control the minimum FoS and the time to minimum FoS. The following parameters were varied one at a time from the baseline values in Table 1: effective cohesion c' (±10%, ±20%), effective friction angle φ' (±1°, ±2°), saturated permeability k_{sat} (×0.1, ×0.5, ×2, ×10), the van Genuchten SWCC parameters α and n (±15% each), and the peak rainfall intensity (30, 45, and 60 mm/h, with the same 72-hour dual-peak pattern). The results are summarized in Table 4 and Figure 8.

The minimum FoS was least sensitive to k_{sat}, which changed it only within about ±3% over the range k_{sat} ×0.1 to k_{sat} ×10 (i.e., one order of magnitude below and above the baseline), but k_{sat} had a strong influence on the time to minimum FoS, which decreased from 58 h at k_{sat} ×0.1 to 31 h at k_{sat} ×10. The SWCC parameters α and n had a modest effect on the minimum FoS (±4–5% for a ±15% change), with α controlling the rate of suction loss and n controlling the shape of the water-retention curve. Peak rainfall intensity had a substantial effect: minimum FoS values were 1.12, 0.94, and 0.86 for peak intensities of 30, 45, and 60 mm/h, respectively, while the time to minimum FoS decreased from 52 h to 34 h as peak intensity increased from 30 to 60 mm/h (a twofold increase).

Overall, the analysis indicates that the minimum FoS of Profile C is governed primarily by the effective friction angle and secondarily by cohesion and peak rainfall intensity, whereas the timing of the minimum FoS is controlled mainly by k_{sat} and peak intensity. These results imply that accurate characterization of φ' and k_{sat} is essential for reliable rainfall-threshold development in residual soil slopes, and they are consistent with the dominant role of hydraulic properties reported by Rahimi et al. (2020). Because this is a deterministic, one-at-a-time sensitivity analysis and not a probabilistic assessment, the discussion of mechanisms in the Discussion section is presented as hypotheses informed by these sensitivities rather than as quantified predictions.

This work is licensed under a Creative Commons Attribution 4.0 International license
Structures, Infrastructure, Planning, Implementation, and Legislation (SIPIL)
Vol. 02, No. 2, October 2026

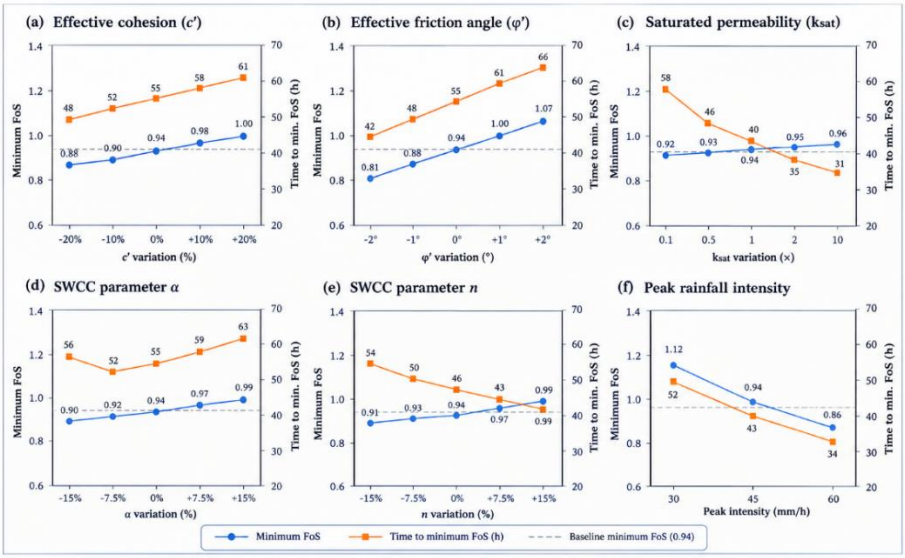


Figure 8. Sensitivity of the minimum FoS and the time to minimum FoS to shear strength, hydraulic, and rainfall parameters

DISCUSSION

The results indicate that the modeled residual soil slopes were sensitive to intense rainfall, primarily because infiltration progressively reduced matric suction in the shallow unsaturated zone, thereby decreasing soil shear strength. This behavior is consistent with previous coupled infiltration–stability studies (Chen et al., 2021; Rahimi et al., 2020). Across the four profiles, the factor of safety (FoS) decreased by 25.0–31.9% relative to the initial (dry/long-term) condition, which is comparable in magnitude to reductions reported for tropical residual soil slopes under coupled seepage–stability analyses (Zhou et al., 2022; Satyanaga et al., 2025). The temporal response varied among profiles, with minimum FoS values occurring between 40 and 58 hours. Profiles A, B, and D reached their minimum FoS at 58, 55, and 50 hours, respectively, whereas Profile C reached its minimum at hour 40.

These differences suggest that slope response depends not only on rainfall intensity but also on initial stability and the rate at which the wetting front reaches the critical slip zone (Table 2). For Profile C, the minimum FoS coincided with the second rainfall peak because the wetting front had already reached approximately 3.2 m, encompassing the critical slip zone at a depth of 3.0 m (within the 1.5–3.0 m range observed across all profiles). The pore-water pressure at the critical slip depth had consequently become slightly positive (+1.5 kPa), indicating that the loss of matric suction and the associated reduction in shear strength had progressed sufficiently to produce the minimum FoS without an additional time lag. The differences in minimum FoS among the profiles were governed largely by their initial stability, although geometry and rainfall-induced hydraulic changes also contributed. Profile C, with an inclination of 38° and a height of 15 m, had the lowest initial FoS (1.38) and reached a minimum FoS of 0.94, indicating predicted instability under the specified design storm. In contrast, Profile A, with an inclination of 25° and a height of 8 m, had the highest initial FoS (1.92) and retained a minimum FoS of 1.44. Profiles B and D reached minimum FoS values of 1.12 and 1.08, respectively, indicating substantially reduced stability margins without crossing the nominal failure threshold of FoS = 1.0 (Table 2).

The relative FoS reductions in Profiles B, C, and D were similar, ranging from 30.3% to 31.9%, whereas Profile A experienced a smaller reduction of 25.0%. This comparison suggests that the lowest minimum FoS in Profile C cannot be attributed solely to a greater percentage loss of stability; its lower

This work is licensed under a Creative Commons Attribution 4.0 International license

initial FoS was also a major contributing factor. As an illustrative comparison, applying a 31.9% reduction to Profile B's initial FoS of 1.61 would yield a minimum FoS of approximately 1.10, above unity. However, this calculation is hypothetical and does not isolate the effects of slope geometry. Because inclination and height increase together across Profiles A–C, their individual contributions cannot be distinguished without additional simulations in which each variable is changed independently (Abishev et al., 2023). The critical slip depth increased from 1.5 m in Profile A to 2.2 m in Profile B and 3.0 m in Profile C, while the corresponding wetting-front depths at minimum FoS were 1.8, 2.5, and 3.2 m, respectively (Table 2).

This correspondence suggests that rainfall-induced instability was associated with wetting-front propagation into the shallow soil zone containing the critical slip surface. Similar relationships between infiltration and slip-surface development have been reported in previous studies of rainfall-induced slope instability (Hou et al., 2021; Mburu et al., 2022). Profile C exhibited both the deepest wetting front and the earliest minimum FoS, suggesting that its geometry and initially lower stability were associated with a more rapid progression toward critical conditions. Nevertheless, the four-profile comparison does not independently establish the effects of slope inclination and height on infiltration rate or failure timing. These relationships should therefore be interpreted as associations within the modeled configurations rather than universal causal relationships. Profile D, which included a toe cut and had a slope inclination of 28° and a height of 10 m, exhibited an initial FoS of 1.55, lower than the value of 1.61 obtained for Profile B despite its gentler inclination and lower height. A simple linear interpolation between the initial FoS values of Profiles A (1.92 at 25°) and B (1.61 at 32°) would yield an estimated FoS of approximately 1.79 at 28°; this interpolation is presented here only as an illustrative reference, not as a model output.

The difference suggests that the toe cut and other geometric differences may have contributed to the lower initial stability of Profile D. However, this estimate is indicative only because slope height, soil thickness, and other geometric characteristics were not held constant. The toe cut may reduce lateral support near the slope base and influence local infiltration and pore-water pressure distributions, but these mechanisms cannot be quantified independently from the present comparison. The similar rainfall-induced FoS reductions in Profiles B and D (30.4% and 30.3%, respectively) further indicate that the toe cut did not produce a clearly distinguishable additional relative reduction under the modeled storm. Accordingly, its influence should be considered a plausible mechanism requiring further investigation rather than a separately quantified effect.

The hydraulic parameters provide further insight into the modeled response. The saturated hydraulic conductivity of the residual soil was 3.6×10^{-6} m/s, equivalent to approximately 13 mm/h, whereas the peak rainfall intensity was 45 mm/h. The computed infiltration flux reached approximately 13 mm/h during peak rainfall, suggesting that the infiltration capacity of the soil limited water entry under those conditions. If the reported flux and rainfall intensity are representative of the same time interval and surface area, the difference would correspond to approximately 32 mm/h of rainfall not entering the soil at that peak, potentially becoming surface runoff or temporary surface storage. This interpretation is consistent with the importance of hydraulic conductivity and storm duration in controlling transient infiltration and slope stability (Rahimi et al., 2020).

The saturated hydraulic conductivity of the saprolite was approximately nine times lower than that of the residual soil, which could favor localized water accumulation near the soil interface. However, pore-water pressure at the residual soil–saprolite boundary reportedly remained negative, between −10 and −15 kPa, throughout the 72-hour storm. This indicates that the interface did not reach positive pore-water pressure under the modeled conditions. Because the critical slip surfaces remained within

This work is licensed under a Creative Commons Attribution 4.0 International license

the residual soil, the results suggest that strength reduction in the shallow, suction-affected layer governed the modeled instability rather than failure along a saturated soil interface (Table 1).

The sensitivity analysis further clarifies the relative importance of the mechanical and hydraulic parameters. For Profile C, changing the effective friction angle by ±2° altered the minimum FoS by approximately ±13.8%, while changing effective cohesion by ±20% produced a change of approximately ±6.4%. Variations of ±15% in the soil-water characteristic curve parameters α and n resulted in changes of approximately 4–5%, whereas saturated hydraulic conductivity had a comparatively small effect on minimum FoS (approximately 3%) but a stronger effect on the time at which the minimum occurred. The minimum FoS also varied with peak rainfall intensity: values of 1.12, 0.94, and 0.86 were obtained for rainfall intensities of 30, 45, and 60 mm/h, respectively. These results indicate that shear-strength parameters and the hydraulic characteristics governing suction loss were important controls on the magnitude of the minimum FoS, while hydraulic conductivity influenced the timing of the response. In particular, the reported change in the time to minimum FoS from 58 hours at 0.1 times the baseline hydraulic conductivity to 31 hours at 10 times the baseline value suggests that changes in infiltration properties can substantially alter the timing of critical conditions.

These findings are consistent with the need to consider both mechanical strength and transient hydraulic behavior when evaluating rainfall-induced slope instability (see Sensitivity Analysis, Section 3.4). The comparison between the three-dimensional finite element method (3D FEM) and two-dimensional limit-equilibrium results showed a difference of 4.8–8.6% under dry conditions. This level of agreement provides a useful consistency check for the dry-condition numerical implementation, although it does not independently validate the model against field observations. The comparison also does not establish whether 3D analysis is more accurate than 2D analysis under rainfall because equivalent transient rainfall simulations were not performed using both approaches. In particular, the potential influence of localized three-dimensional infiltration near the toe cut of Profile D remains a hypothesis that requires direct testing using comparable 2D and 3D hydraulic boundary conditions. Previous studies have highlighted the potential relevance of three-dimensional analysis for slopes with complex geometries, layered soils, and non-uniform infiltration patterns (Zhou et al., 2022; Jiang et al., 2022).

Further comparative simulations are needed to determine whether these effects materially change predicted pore-water pressures, critical slip surfaces, or minimum FoS under rainfall. Several limitations should be considered when interpreting these findings. First, the numerical model was not validated against monitored pore-water pressures or a documented slope failure; therefore, the absolute FoS values and predicted times of minimum stability should be interpreted as model-based estimates rather than verified field outcomes. Second, the analysis considered only four slope profiles and one synthetic 72-hour design storm. The results cannot therefore be generalized directly to all tropical hilly areas or to storms with different temporal patterns and antecedent moisture conditions. Third, spatial variability in soil properties, soil-water characteristic curve hysteresis, and vegetation-root reinforcement were not incorporated, although these factors may influence infiltration and slope resistance (Das et al., 2023; Jiang et al., 2022; Oguz et al., 2022; Mburu et al., 2022).

Finally, the deterministic analysis did not quantify uncertainty in the input parameters or the predicted stability outcomes. Future research should incorporate field monitoring, additional rainfall scenarios, and probabilistic analyses to evaluate the robustness of the predicted FoS values and failure timing. The observed relationships among cumulative rainfall, wetting-front depth, and minimum FoS may also inform the development of rainfall-based early-warning criteria. However, no operational warning threshold can be established from the present results alone.

This work is licensed under a Creative Commons Attribution 4.0 International license

CONCLUSIONS

This study developed a 3D finite element model coupling transient unsaturated seepage analysis with the shear strength reduction method to assess residual soil slope stability under an extreme rainfall event. Across four representative slope profiles (25°–38° inclination, 8–15 m height), a 72-hour design rainfall with a peak intensity of 45 mm/h caused pore-water pressure in the residual soil layer to rise from an initial suction of approximately −55 kPa toward near-zero or slightly positive values within 24–48 hours, and reduced the 3D FoS by 25.0–31.9% relative to the initial (dry/long-term) condition. The steepest profile (38°, H = 15 m) reached a minimum FoS of 0.94 after approximately 40 hours, and all four profiles showed a shallow critical slip surface (1.5–3.0 m) within the residual soil layer, indicating that shallow rainfall-triggered failure is the dominant mechanism for the modeled profiles.

The 3D FEM results were 4.8–8.6% higher than 2D limit-equilibrium calculations for the dry condition, which verifies the model under dry conditions but does not validate the transient rainfall response. These findings are based on four profiles and one synthetic rainfall event and cannot be generalized directly to the entire tropical hilly region. They provide a basis for future development of rainfall thresholds for slope stability assessment in hilly residual soil terrain; they are not themselves an early-warning threshold. Future work should include validation against field monitoring or observed failures, a 2D versus 3D comparison under rainfall, and probabilistic rainfall and spatially variable soil property scenarios.

REFERENCES

Abishev, R., Satyanaga, A., Sharipov, A., Wijaya, M., Hamdany, A. H., Moon, S.-W., & Kim, J. (2023). Effect of slope geometry on stability of slope in Almaty. E3S Web of Conferences, 382, 13005. https://doi.org/10.1051/e3sconf/202338213005

Bentley Systems Inc. (2023). PLAXIS 3D reference manual. Bentley Systems.

Cai, F., & Ugai, K. (2004). Numerical analysis of rainfall effects on slope stability. International Journal of Geomechanics, 4(2), 69–78. https://doi.org/10.1061/(ASCE)1532-3641(2004)4:2(69)

Chai, J., Shen, S. L., & Ding, W. (2020). Analysis of rainfall-induced slope instability using coupled seepage-deformation finite element method. Computers and Geotechnics, 118, 103340.

Chen, Y., Irfan, M., Uchimura, T., Cheng, G., & Nie, W. (2021). Influence of rainfall infiltration on pore water pressure and factor of safety for residual soil slope: A case study. Environmental Earth Sciences, 80, 138. https://doi.org/10.1007/s12665-021-09428-4

Das, G. K., Ng, C. W. W., & Zhou, C. (2023). Effects of spatial variability of hydraulic conductivity on rainfall-induced slope failure. Soil Dynamics and Earthquake Engineering, 173, 108157.

Fredlund, D. G., Rahardjo, H., & Fredlund, M. D. (2021). Unsaturated soil mechanics in engineering practice (2nd ed.). Wiley.

Garcia, E. F., Oka, F., & Kimoto, S. (2021). Multiphase coupled elasto-viscoplastic finite element analysis of rainfall infiltration into unsaturated soil slopes. Computers and Geotechnics, 137, 104276.

Hou, X., Vanapalli, S. K., & Li, T. (2021). Water infiltration characteristics in unsaturated soil slopes under rainfall condition. Bulletin of Engineering Geology and the Environment, 80, 3489-3504.

Jiang, S. H., Huang, J., Griffiths, D. V., & Deng, Z. P. (2022). Advances in reliability and risk analyses of slopes in spatially variable soils: A state-of-the-art review. Computers and Geotechnics, 141, 104498.

Kim, J., Hwang, W., & Kim, Y. (2024). Three-dimensional numerical modelling of rainfall-induced shallow landslide in weathered residual soil slope. Landslides, 21, 921-938.

This work is licensed under a Creative Commons Attribution 4.0 International license

Mburu, J. W., Rahardjo, H., & Satyanaga, A. (2022). Effect of hysteresis of soil-water characteristic curve on slope stability analysis under rainfall infiltration. Journal of Rock Mechanics and Geotechnical Engineering, 14(5), 1591-1603.

Muntohar, A. S., Ikhsan, J., Liao, H.-J., Jotisankasa, A., & Jetten, V. G. (2022). Rainfall infiltration-induced slope instability of the unsaturated volcanic residual soils during wet seasons in Indonesia. Indonesian Journal on Geoscience, 9(1), 71–85.

Ng, C. W. W., & Menzies, B. (2020). Advanced unsaturated soil mechanics and engineering (2nd ed.). CRC Press.

Nian, T.-K., Huang, R.-Q., Wan, S.-S., & Chen, G. (2012). Three-dimensional strength-reduction finite element analysis of slopes: Geometric effects. Canadian Geotechnical Journal, 49(11), 1291–1304.

Oguz, E. A., Depina, I., & Thakur, V. (2022). Effects of soil heterogeneity on susceptibility of shallow landslides: 3D probabilistic slope stability analysis. Engineering Geology, 296, 106465.

Rahardjo, H., & Satyanaga, A. (2019). Slope stability assessment of residual soil slope under rainfall infiltration. In Geotechnics for Sustainable Infrastructure Development. Springer.

Rahimi, A., Rahardjo, H., & Leong, E. C. (2020). Effect of hydraulic properties of soil on rainfall-induced slope failure. Engineering Geology, 269, 105546.

Satyanaga, A., Aventian, G. D., Rahardjo, H., Huang, W., & Hutama, D. A. (2025). Experimental and numerical approaches for assessing the stability analyses of shallow residual soil slopes. International Journal of Geotechnical Engineering, 19(6), 382-399. https://doi.org/10.1080/19386362.2025.2506553

Setiawan, B., & Pratama, A. (2022). Numerical analysis of residual soil slope stability under extreme rainfall in hilly terrain of West Sumatra, Indonesia. IOP Conference Series: Earth and Environmental Science, 1041, 012025.

Sharma, L. K., Umrao, R. K., Singh, R., Ahmad, M., & Singh, T. N. (2021). Geotechnical characterization of road-cut hill slope forming unconsolidated geomaterials in tropical hilly terrain. Geotechnical and Geological Engineering, 39, 503-515.

Su, Z., & Shao, L. (2021). A three-dimensional slope stability analysis method based on finite element method stress analysis. Engineering Geology, 284, Article 105910. https://doi.org/10.1016/j.enggeo.2020.105910

Tohari, A., Nishigaki, M., & Komatsu, M. (2007). Laboratory rainfall-induced slope failure with moisture content measurement. Journal of Geotechnical and Geoenvironmental Engineering, 133(5), 575–587. https://doi.org/10.1061/(ASCE)1090-0241(2007)133:5(575)

Tozato, K., Dolojan, N. L. J., Touge, Y., Kure, S., Moriguchi, S., Kawagoe, S., Kazama, S., & Terada, K. (2022). Limit equilibrium method-based 3D slope stability analysis for wide area considering influence of rainfall. Engineering Geology, 308, Article 106808. https://doi.org/10.1016/j.enggeo.2022.106808

Wang, L., Sun, D., & Li, P. (2023). Back analysis of rainfall-induced colluvial slope failure using coupled seepage-strength reduction finite element method. Bulletin of Engineering Geology and the Environment, 82, 421.

Yang, S.-R., & Huang, L.-J. (2023). Infiltration and failure behavior of an unsaturated soil slope under artificial rainfall model experiments. Water, 15(8), Article 1599. https://doi.org/10.3390/w15081599

This work is licensed under a Creative Commons Attribution 4.0 International license

Yudhistira, D., Hakim, M., & Wibowo, S. (2024). Slope stability analysis using Plaxis and Slope/W: Case study of Bagbagan-Jampangkulon road section. IOP Conference Series: Earth and Environmental Science, 1321, 012031.

Zhan, T. L. T., Ng, C. W. W., & Fredlund, D. G. (2013). An analytical solution for rainfall infiltration into an unsaturated infinite slope and its application to slope stability analysis. International Journal for Numerical and Analytical Methods in Geomechanics, 37(12), 1737–1760. https://doi.org/10.1002/nag.2106

Zhan, T. L., Jia, G. W., Chen, Y. M., Fredlund, D. G., & Li, H. (2020). An analytical solution for rainfall infiltration into an unsaturated infinite slope. International Journal for Numerical and Analytical Methods in Geomechanics, 45(6), 726-747.

Zhou, C., Ng, C. W. W., & Chen, R. (2022). A three-dimensional finite element analysis of rainfall-induced slope instability incorporating a fully coupled hydro-mechanical model. Canadian Geotechnical Journal, 59(4), 543-556.